University of Groningen

Binding of Helium to Metallic Impurities in Tungsten; Experiments and Computer Simulations

Kolk, G.J. van der; Veen, A. van; Caspers, L.M.; De Hosson, J.T.M.

IMPORTANT NOTE: You are advised to consult the publisher's version (publisher's PDF) if you wish to cite from it. Please check the document version below.

Document Version
Publisher's PDF, also known as Version of record

Publication date:
1985

Link to publication in University of Groningen/UMCG research database

BINDING OF HELIUM TO METALLIC IMPURITIES IN TUNGSTEN; EXPERIMENTS AND COMPUTER SIMULATIONS

G.J. van der KOLK [1,3], A. van VEEN [1], L.M. CASPERS [1]* and J.Th.M. de HOSSON [2]

[1] *Delft University of Technology/Interuniversity Reactor Institute, Mekelweg 15, 2629 JB Delft, The Netherlands*
[2] *University of Groningen, Materials Science Centre, Nijenborgh 18, 9747 AG Groningen, The Netherlands*
[3] *Present address;Philips Research Laboratories, 5600 JA Eindhoven, The Netherlands*

A W(100) single crystal was implanted with low doses Ag, Cu, Mn, Cr, Al or In. Subsequent heating to 1600 K removed all vacancies and left the implants in substitutional positions. Low energy He was injected, and binding of He to the substitutional impurities was observed. Binding energies were found as high as 1.25 eV for one He atom. Pair potential calculations were performed; the calculated binding energies correspond reasonably with the measured ones.

1. Introduction

In future fusion reactors the first wall limiting the plasma will be subjected to high fluences of fast particles escaping from the plasma e.g., hydrogen isotopes and ^{4}He. At the same time the build up of an appreciable concentration of H and He via the transmutation reactions (n.p) and (n, α) is envisaged. It has been shown that clustering of He plays an important or even decisive role in, the process that leads to intolerable modification of the first wall (e.g. blistering, swelling). Recently Helium Desorption Experiments (HDS) combined with electron microscopy have improved the insight into the early phase of the he clustering process [1,2]. Various experiments have beeen performed on low-energy and low-dose He implantation in among others single crystals of W, Mo and Ni [3–6]. In these experiments it was demonstrated that He binds to lattice vacancies with high binding energies. The binding of He to heavier substitutional noble gases was also observed [7]. It was found that the larger the substitutional noble gas atom the smaller the He-binding energy. A very important result of THDS experiments was that once the first He is bound to a substitutional heavy noble gas atom, the second He atom will be bound more tightly.

It was observed that in Mo this general trend holds for up to at least 1000 He atoms per trap. So any

trapping centre for He will act as a nucleation centre for bubbles.

Although tungsten is no candidate material for the first wall of the early generation of fusion reactors, tungsten was studied here, because W or Mo will probably be used in plasma limiters, divertors etc. [8].

Small amounts of the metallic impurities Ag, Cu, Mn, Cr, Al and In are introduced in a W(100) single crystal by 5 keV ion implantation. In all cases annealing at 1600 K is sufficient to evaporate the excess vacancies around the implants so that substitutionality of the implants is ensured. In section 3 it is found that He is bound by the metallic impurities Al, Cr, Ag, Mn and Cu with binding energies ranging from 0.75 eV to 1.25 eV. In section 4 a model is applied which calculates He binding energies from differences in local electron densities. In section 5 the experimental results and the results of the model calculations are compared and discussed.

2. Experimental

The equipment used in this study has already been described in refs. [9,10]. Basically the equipment consists of a large UHV target chamber being held at a pressure of 2×10^{-8} Pa. In the centre of the chamber a W(100) high purity single crystal is mounted. The sample can be heated by 1.5 keV electron bombardment on the rear. A WRe3%–WRe25% thermocouple is used to

---

* Sadly Dr. L.M. Caspers died during the course of this work.

measure the temperature of the crystal during computer controlled linear heating with time (the heating rate normally used is 40 K/s). Auxiliary devices are a gas ion source with which low energy He implantation is performed (standard energy 250 eV), a quadrupole mass analyser equipped with an electron multiplier to detect desorbing He, and a metal ion source (5–30 keV acceleration voltage). In the beam line of the metal ion source magnetic deflection over 90 degrees ensures adequate mass separation for our purpose. Both in the gas ion beam and the metal ion beam electrode pairs are mounted which enable sweeping of the beams to provide a uniform distribution of the ions on the crystal surface. The W(100) single crystal is the same as has been used in ref. [10].

The standard experimental procedure adopted for this study was to bombard the crystal with 2×10^{12} 5 keV metal ions cm^{-2}. The angle of incidence with respect to the surface normal was about 15 degrees. Following the metal implantation the target was annealed to a certain temperature with a heating rate of 40 K/s. Subsequently 3×10^{12} 250 eV He^+ cm^{-2} was injected perpendicularly to the surface. He desorption was monitored by the quadrupole mass analyser mentioned above during linear heating with time. The thus obtained spectra were corrected for the residence time τ of He in the desorption volume.

3. Experimental results

3.1. Annealing temperature variation after metal implantation

In fig. 1 helium desorption spectra are shown for W(100) implanted with 2×10^{12} 5 keV Ag^+ cm^{-2}, annealed to the indicated temperatures and subsequently injected with 3×10^{12} 250 eV He^+ cm^{-2}. The peaks labelled H and G are attributed to He release from monovacancies, see ref. [3]. We attribute the peaks labelled A, B and C to He desorbing from substitutional Ag atoms. In section 3.2 this will be elucidated. In fig. 2 the peak populations versus annealing temperature are shown for the G and H peak and the A, B and C peaks. At around 800 K a steep decrease of the G and H peak population is seen which we attribute to stage III recovery. The empty vacancies become mobile and recombine at the near surface thereby being lost as traps for He. It can be seen that in the same temperature region the A, B and C peaks grow. In ref. [11] it is shown that the suppression of the A, B and C peaks at annealing temperatures below 800 K can be attributed to effects
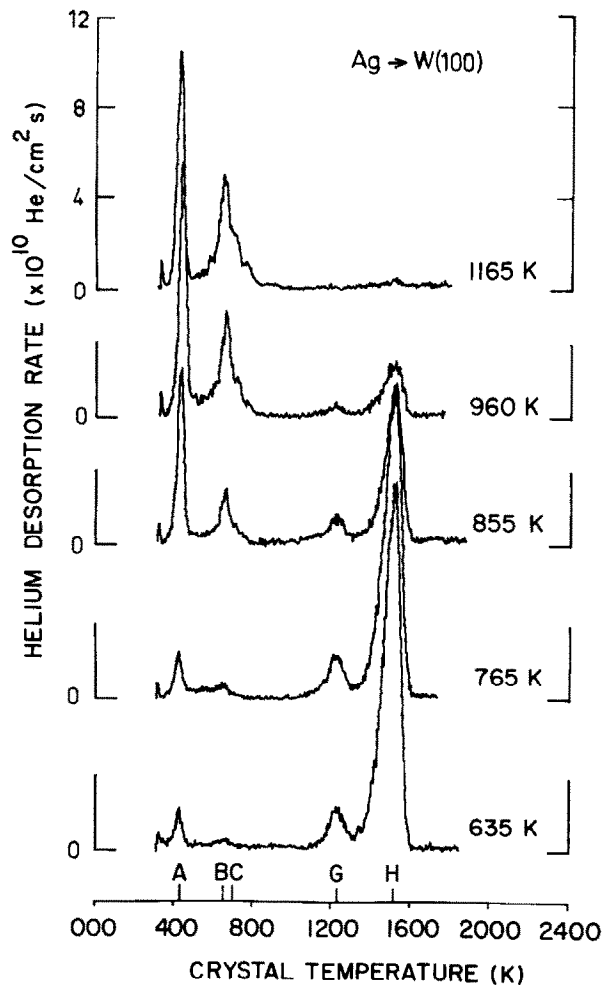

Fig. 1. Helium desorption spectra for W(100) implanted with 2×10^{12} 5 keV Ag^+ cm^{-2}, annealed to the indicated temperatures and subsequently injected with 3×10^{12} 250 eV He^+ cm^{-2}.
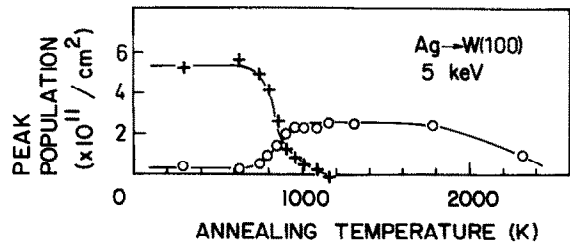

Fig. 2. Peak populations as a function of annealing temperature, Bombardment parameters as in fig. 1 (+) sum of G and H, (O) sum of A, B and C.

caused by vacancies situated within a distance not larger than 3 lattice constants from the implants. Both shielding of substitutional Ag (AgV) by vacancies (V) for migrating He as well as He drainage to and retrapping in nearby vacancies during desorption from AgV occur. Once the nearby vacancies have become mobile a large fraction of them will be trapped by the metal atoms. However the binding energy is so low that at temperatures slightly beyond stage III they will be detrapped and released. For all metallic implants a similar annealing behaviour was found; after 5 keV implantation vacancy type traps disappear at stage III at the same annealing temperature as where the A, B and C peaks appear. It is seen that between 1000 and 1800 K the population of the peaks does not change. This is found to be true for all implants, therefore annealing up to 1600 K ensures that the impurity is in a single state (substitutional) and still does not move out of the crystal by diffusion.
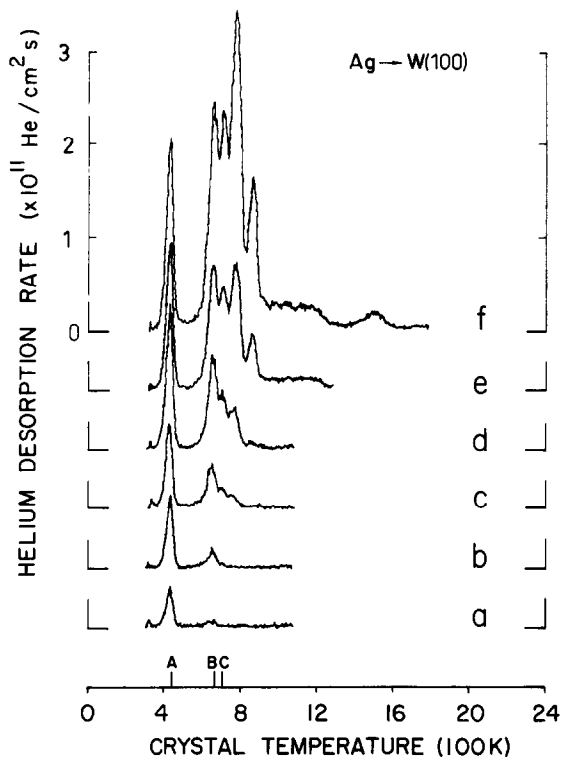
3.2. Peak assignment

In fig. 3 helium desorption spectra are shown for W(100) implanted with different metallic impurities, annealed up to 1600 K and injected with the indicated doses of 250 eV He^+. It is seen that for most implants the peak profile is similar, the peak temperatures depend a little on the implanted species. It should be noted that in the case of In implantation no peaks are visible, indicating that the binding energy of He to substitutional In is too low to permit permanent binding at room temperature. Beside the A, B and C peaks already observed in the previous section extra peaks are seen to develop at temperatures above the C peak. The peak populations of the Ag implanted series are shown in fig. 4. it should be noted that due to the low desorption temperature the first peak shown here was not detected in earlier experiments [10]. The peak evolution as a function of He dose corresponds with the behaviour expected for traps which bind He with increas-

Fig. 3a. Desorption spectra of W(100) bombarded with 2×10^{12} 5 keV Ag^+ cm^{-2}, annealed to 1600 K and injected with 250 eV He^+, doses are (a) 6.5×10^{11} cm^{-2}; (b) 1.5×10^{12} cm^{-2}; (c) 3×10^{12} cm^{-2}; (d) 6×10^{12} cm^{-2}; (e) 1.2×10^{13} cm^{-2}; (f) 2.4×10^{13} cm^{-2}.

Fig. 3b. As in fig. 3a, but for Mn^+, He doses are (a) 1.7×10^{12} cm^{-2}; (b) 3.4×10^{12} cm^{-2}; (c) 5.2×10^{12} cm^{-2}; (d) 8.6×10^{12} cm^{+2}.

Fig. 3c. As in fig. 3a, but for Al^+, He doses are (a) 1.3×10^{12} cm^{-2}; (b) 3×10^{12} cm^{-2}; (c) 6×10^{12} cm^{-2}; (d) 1.2×10^{13} cm^{-2}.
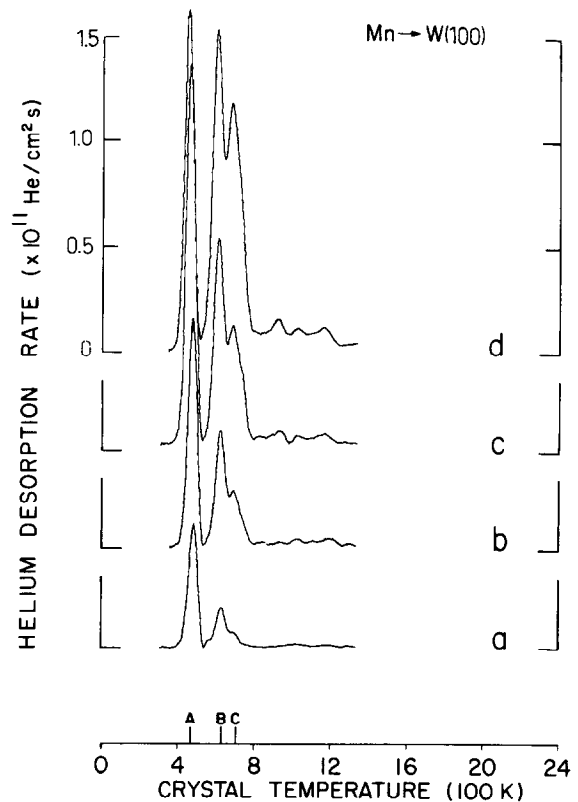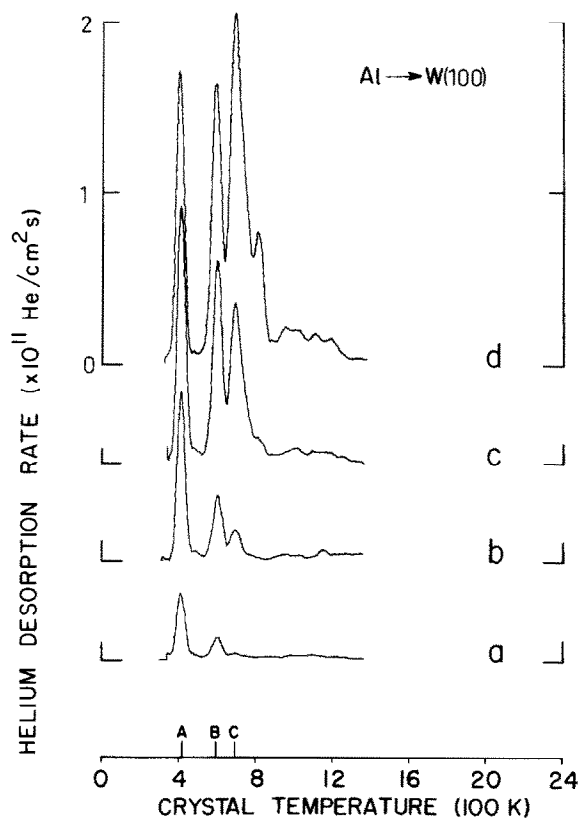

Fig. 3d. As in fig. 3a, but for Cu^+, He doses are (a) 1×10^{12} cm^{-2}; (b) 2×10^{12} cm^{-2}; (c) 3.2×10^{12} cm^{-2}; (d) 5.8×10^{12} cm^{-2}; (e) 7.5×10^{12} cm^{-2}.

ing binding energies. Trapping of one He atom by a trap should increase linearly with dose, a peak representing trapping of 2 He atoms should increase approximately quadratic. Furthermore, since the second He atom is bound more strongly than the first one, two He atoms will be released once the dissociation temperature for the second He atom is attained. Thus for higher He doses the B peak will be higher than the A peak. The peak evolution can be calculated with a model described in [12]. The trap distribution, the capture constant for He trapping and the He range are model parameters. With the model the depth dependent stationary He concentration is calculated applying diffusion theory to the initial He range. From the thus obtained stationary He distribution and given trap distribution He trapping probabilities and thus peak populations as a function of He dose are obtained. The best fit is shown in fig. 4 (drawn curves). For this fit it had to be assumed that one He desorbs in the A peak, two in
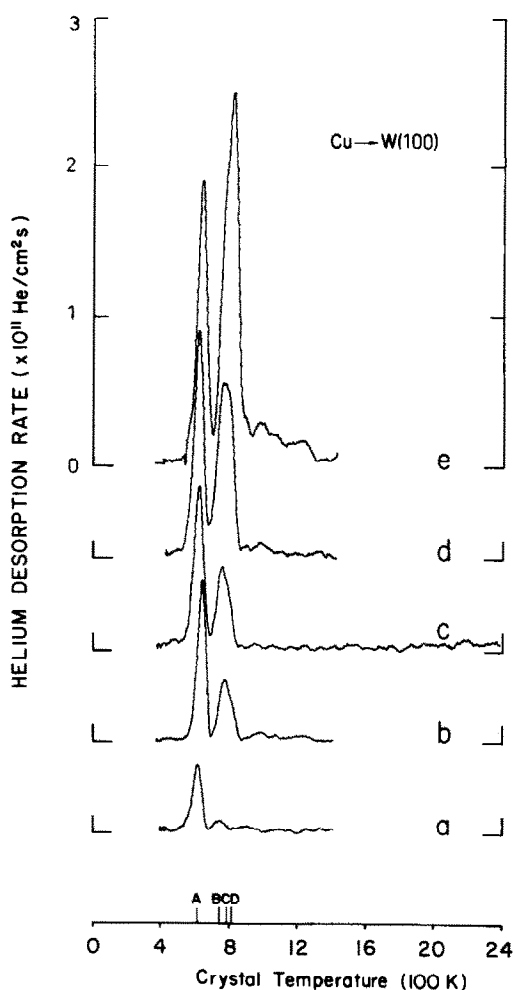
the B peak and three in the C peak. The drawn curves were calculated for an average He penetration depth of 60 Å, an entrance probability of 0.85 [13] and a capture constant of 1.15 [14]. The average depth of Ag was taken as 30 Å, the Ag distribution is shown in the inset of fig. 4. Binary collision simulations with the programme Marlowe predict a rather broad Gaussian distribution with an average depth of 18 Å or 63 Å for 5 keV Ag implanted into W(100) at angles of respectively 20 or 10 degrees off the surface normal. The number of traps which had to be substituted in the model calculations to obtain a reasonable fit with the experimental data was 8.3×10^{11} cm^{-2}.
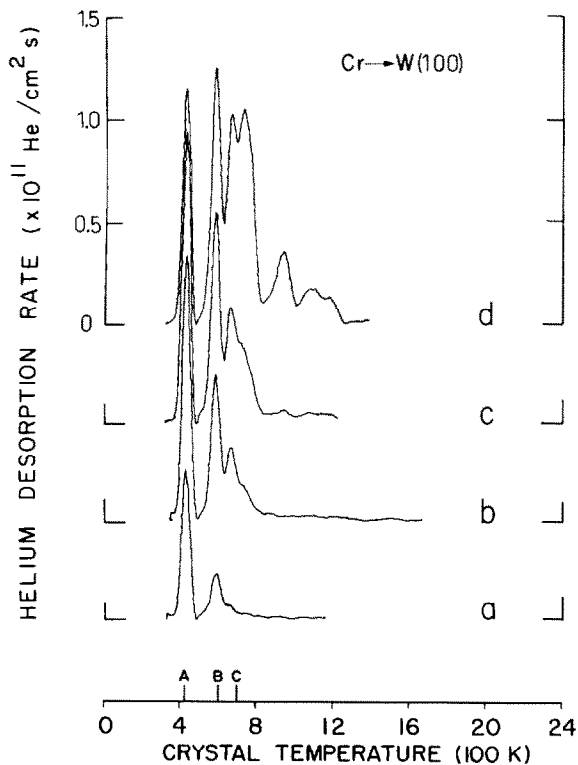
Fig. 3e. As in fig. 3a, but for Cr^+, He doses are (a) 1.7×10^{12} cm^{-2}; (b) 4×10^{12} cm^{-2}; (c) 6×10^{12} cm^{-2}; (d) 1.2×10^{13} cm^{-2}.

Fig. 4. Individual peak populations as a function of He dose for Ag implanted W, bombardment and annealing parameters as in fig. 3a. (O) peak A, (+) peak B, (x) peak C, (△) other peaks, (−) total. Drawn curves are calculated for a He range of 60 Å, and the Ag distribution shown in the inset. For details see text.
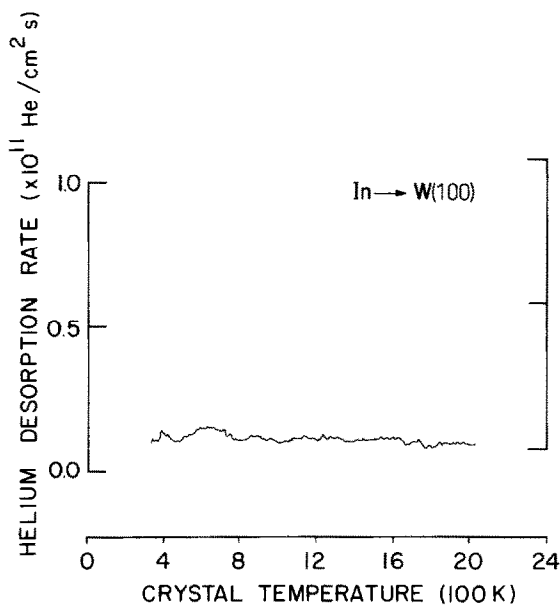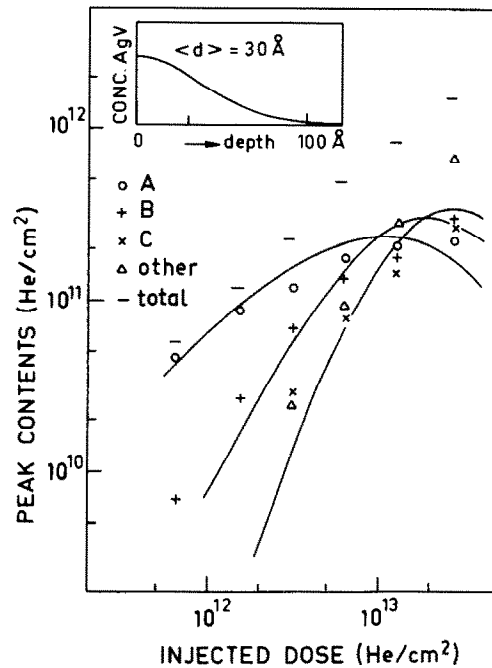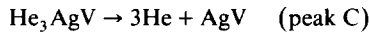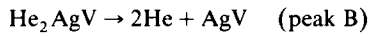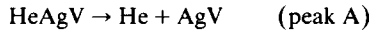
Fig. 3f. As in fig. 3a, but for In^+, He dose is 3×10^{12} cm^{-2}.

Sticking probabilities for 5 keV Kr and Xe on W were reported to be about 0.6 to 0.7 [15]. We expect the same sticking probability for Ag. The heating to 1600 K applied in this study will have removed a fraction of the Ag atoms of 0.3 as well. So the number of traps deduced from the peak populations is in fair agreement with what is expected for the implanted dose of 2×10^{12} 5 keV Ag^+ cm^{-2}.

In the next lines we will argue that the implanted impurity atoms are located in substitutional positions. (i) According to an empirical rule formulated by Sood [16] an implanted species will be in a substitutional position if: (a) the atomic radius is within -15% and $+40\%$ of that of the host, and (b) the electronegativity according to the Gordy scale [17] is within 0.7 of the electronegativity of the host. For all implants except In this is the case. (ii) Further experimental evidence follows from the desorption spectra. All vacancy type traps are removed after annealing to above stage III, see the previous section. For all implants except In the behaviour was totally analogous to He binding to substitutional Ar, Kr and Xe. Substitutionality of the noble gas

implants after annealing was proven experimentally [18,19]. The binding energy observed here for the first He atom is of the same magnitude as that of He to KrV (1.7 eV) or to XeV (1.2 eV) in tungsten. Furthermore the feature that the second and third He atom are stronger bound than the first in the case of substitutional Ar, Kr and Xe holds for the metallic impurities as well.

Having established that the trap is a substitutional Ag atom, we make the following peak assignments:

$$HeAgV \rightarrow He + AgV \quad \text{(peak A)}$$
$$He_2AgV \rightarrow 2He + AgV \quad \text{(peak B)}$$
$$He_3AgV \rightarrow 3He + AgV \quad \text{(peak C)}$$

The peaks emerging at higher He doses will correspond with dissociation of more than 3 He atoms from a Ag atom.

For all other implants except In similar peak patterns were found with a similar peak evolution as a function of He dose for the A, B and C peaks. So peak assignments as above can be made, but for Ag is X, with X = Al, Cr, Cu and Mn.

3.3. Peak fitting

Helium desorption peaks from simple defects with a low concentration and low helium filling can be described by a single step dissociation process followed by diffusion to the surface. In W at room temperature the first process is dominant due to the low interstitial migration energy for He of 0.3 eV [20,21]. Therefore the He release rate $R(t)$ can be described by the formula:

$$R(t) = \nu_0 c(t) \exp(-E^d/kT(t)) \tag{1}$$

with $c(t)$ the concentration of He filled defects at time t, E^d the dissociation energy, ν_0 the zero temperature jumping frequency, k the Boltzmann factor and $T(t)$ the temperature at time t. In principle E^d and ν_0 can be derived from a single experiment by matching the observed peak with a numerically obtained solution of eq. (1). In fig. 5 several fitting curves are shown for an A peak of Ag in W. For a fixed value of ν_0 values of E^d were chosen so that the left side of the peak was fitted well. It can be seen that the calculated peak for $\nu_0 = 5 \times 10^{11}$ s^{-1} is too broad whereas the others are too narrow. The accuracy of this method is limited; ν_0 is estimated to be between 5×10^{11} and 5×10^{13} s^{-1}. In this particular case the peak suffered only a minimal shape distortion; the average residence time τ of He in the mass spectrometer volume was quite short (< 0.05 s) and the width of the peak in the time domain rather large

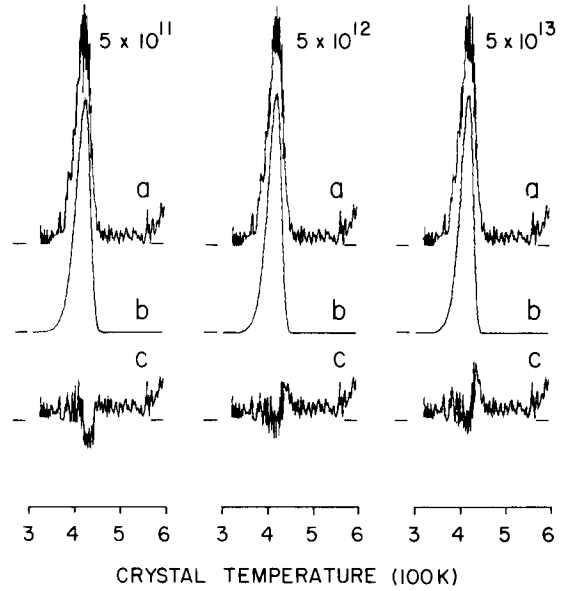Fig. 5. Comparison between the A peak of W(100), implanted with 2×10^{12} 5 keV Ag$^+$ cm^{-2}, annealed to 1600 K and injected with 3×10^{12} 250 eV He$^+$ cm^{-2} (heating rate is 20 K/s), and calculated peaks. (a) spectrum; (b) calculated peak; (c) difference of (a) and (b).

relative to τ due to the low heating rate ($\beta = 20$ K/s). Despite of this we were unable to match the peak perfectly, the residual of the measured peak after subtraction of the calculated peak always showed a small deviation at the high temperature side of the peak. This can be understood in the following way. There is a small fraction of He entering small volumes where the average pumping speed will be much lower, thus leading to a larger average residence time for a fraction of the He atoms. This will enlarge the tail of the peak.

An alternative method for obtaining ν_0 is to extract the maximum peak temperature T_m for different linear heating rates β. The following equation should be fulfilled under the assumption that ν_0 is independent of temperature:

$$\frac{E^d}{kT_m} = -\ln \frac{\beta E^d}{\nu_0 kT_m^2}. \tag{2}$$

A plot of $\ln \beta/T_m^2$ versus $1/T_m$ should be a straight line from which both E^d and ν_0 can be determined. Fig. 6 shows such a plot for the A peak in the desorption spectrum of Ag implanted W.

The errors in the dissociation energy and the jumping frequency are mainly determined by three effects.
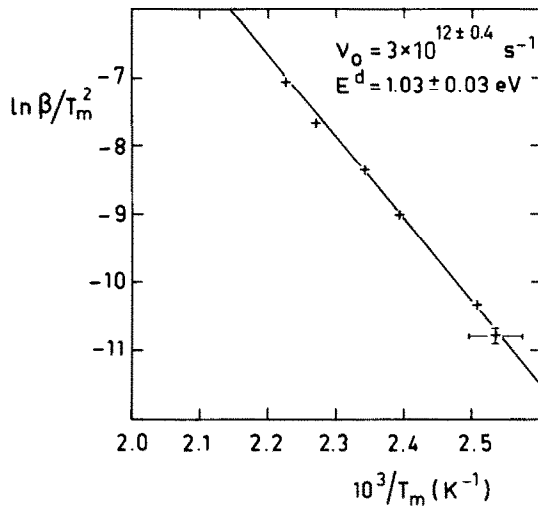
Fig. 6. Plot of $\ln \beta/T_m^2$ versus $1/T_m$ for the A peak observed for Ag implanted W.

The largest error is introduced by the uncertainty of the temperature of the cold joint of the thermocouple which is inside the UHV chamber. Especially at the low peak-temperatures in this study this can introduce an error of 1.5% in the absolute value of T_m. Another error may be introduced by the data acquisition system. This error was kept within 0.5%. The error in the thermocouple is according to the manufacturer less than 1%. A small error is introduced by fluctuations of the heating rate β. For spectra with β below 80 K/s this error was estimated to be less than 3%. Differentiation of relation (2) with respect to the different physical parameters shows that for the uncertainties quoted above the errors in E^d and $\ln \nu_0$ are largely determined by the uncertainty of T_m and are 3%. The best fit (least square analysis) is shown in the figure. The result is that $E^d = 1.03 \pm 0.03$ eV and $\nu_0 = 3 \times 10^{12 \pm 0.4}$ s^{-1}. These data agree with the

peak fitting results in fig. 5. Furthermore the result is in line with the expected frequency which should be approximately the same as the Debye frequency (for W $\sim 8 \times 10^{12}$ s^{-1}) since He dissociation from substitutional atoms is likely to be governed by vibrations in the surrounding lattice. Peak fitting of results for other implants showed no deviations from the jumping frequency found above, therefore all dissociation energies given in table 1 are based on a value of ν_0 of 3×10^{12} s^{-1}.

3.4. He precipitation at high dose He injection

It was shown recently with HDS that substitutional noble gas atoms in tungsten act as non-saturable traps for helium. The non-saturable traps could be grown with non-damaging low energy He into helium-precipitates containing up to 150 He atoms [7,1]. Injection of 250 eV He up to very high doses in W(100) bombarded with 5 keV Ag and annealed up to 1600 K showed that the He binding energy continues to increase with increasing filling degree. The spectra are similar to those obtained by Kornelsen and van Gorkum [7] on substitutional Ne, Ar, Kr and Xe in W for similar filling degrees. Two spectra are shown in fig. 7; the A, B and C

Table 1
Experimentally derived dissociation energies (eV) for He from implanted impurities in W, ν_0 was taken 3×10^{12} s^{-1}

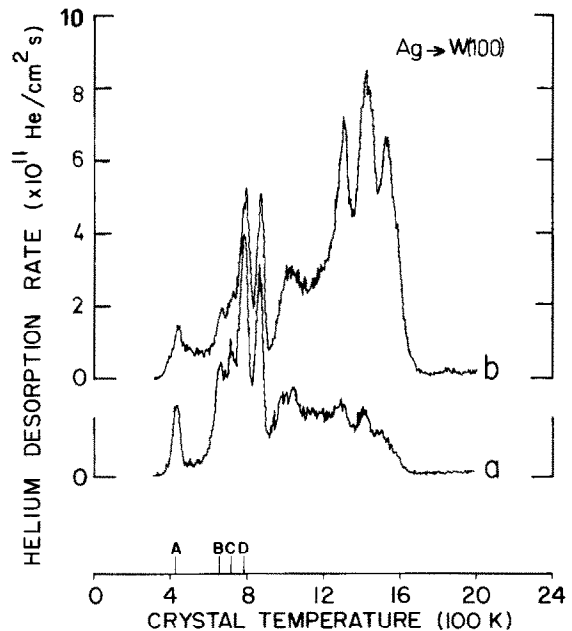| Implant	Peak A	Peak B	Peak C
Ag	1.03 ± 0.03	1.57	1.71
Cu	1.48	1.79	1.88
Al	0.99	1.46	1.69
Mn	1.13	1.51	1.70
Cr	1.02	1.41	1.61
In	< 0.90		

Fig. 7. Spectra of W bombarded with 2×10^{12} 5 keV Ag$^+$ cm^{-2}, heated to 1600 K and injected with 250 eV He$^+$, doses are (a) 6×10^{13} cm^{-2}; (b) 1.2×10^{14} cm^{-2}.

peaks are still visible, but most of the He is trapped with high binding energies. The three large peaks at higher temperature are identical with the peaks found by ref. [7] for a He occupancy per trap ranging from 20 to 90 He atoms.

For the other metallic implants except In similar He precipitation at higher He doses takes place (the first He atom does not bind to In in W at room temperature).

4. Static lattice calculations

4.1. Pair potentials

Static lattice calculations were performed using a model in which a small crystallite of $13 \times 13 \times 13$ a_0^3, containing a defect in the centre, is allowed to relax to the lowest energy. The method is described in ref. [22]. The interaction between two atoms is described with a two-body interaction function, the pair-potential. The results rely on a proper choice of pair potentials. For the W–W potential the potential derived by Johnson and Wilson [23] was used. This potential is based on elastic constants and gives a suitable estimation of the displacement of lattice atoms on which a force is exerted. The He-metal potentials were calculated using a program of Baskes [24], in which the modified Wedepohl method [25,26] is used to derive the pair potential from the radial electron density obtained with Hartree–Fock–Slater calculations (see ref. [27]). The He-metal pair potentials calculated this way predict He-vacancy binding energies for Mo and W which are in close agreement with recent Helium Desorption measurements; the predicted dissociation energies are respectively 4.19 and 4.75 eV, the experimental values are 3.8 ± 0.2 and 4.64 ± 0.04 eV respectively.

The W–X potential with X the impurity was not available in literature, therefore an approximation had to be found which described the correct relaxation of the impurity atom in the vacancy with a He atom bound to it. In view of the noble gas results it is clear that the size of the impurity plays a role. The size of the impurity is largely determined by its atomic volume in pure form. For most alloys a volume contraction is observed relative to the volumes of the alloying components. Therefore in this section a correction will be applied to the atomic volume of X.

In short the method applied was scaling of the W–W potential to a potential representing a bcc X–X interaction. The average between pure W–W and the thus calculated X–X potential was taken to obtain the X–W potential. This approach seems to be quite crude; how-

ever results obtained by Machlin, Maeda and Vitek [28–31] suggest that it might work satisfactorily for some problems. The different steps will be discussed below. Both the potential range and the potential minimum must be scaled.

To adapt the potential range of the W–W potential, so that a X–X potential is obtained, the radii of X and W should be compared. Often half the first neighbour distance is taken as the radius of an atom, in our case however atoms of unlike structure were placed in a bcc structure. Therefore first of all a correction should be made for forcing the atoms in a bcc structure. Machlin [28] has estimated these size corrections, his values were applied in this study. According to several authors the volume contraction upon alloying depends on the difference in electronegativity of the two constituents [28,30,31]. A formula describing this contraction given in ref. [29] and which will be used in this study is as follows:

$$D^{\alpha *} = \frac{D^\alpha}{\left[1 - 0.75 S_\alpha t_{\beta \to \alpha}/(X_\alpha - 0.5)\right]} \quad (3)$$

with D^α the nearest neighbour distance of α (in a bcc structure in our case), $D^{\alpha *}$ is the corrected nearest neighbour distance, S_α is the screening constant tabulated in [28], and $t_{\beta \to \alpha}$ the charge transfer from element β to element α, X_α is the electronegativity of α according to Gordy [17]. Since in our case a very diluted alloy is concerned of X in W the charge transfer of neighbouring W atoms should be minus 1/8 of the charge transfer of X to preserve electroneutrality. From relation (3) D^{X*} and D^{W*} follow. To rescale W–W into W–X the potential range was scaled with the following factor: $f = (D^{X*} + D^{W*})/2D^W$.

To scale the potential minimum a variety of physical parameters as cohesive energy, vacancy formation energy and bulk modulus can be taken. In this context however it should be realized that the Johnson–Wilson W–W potential belongs to a class of potentials which do not aim to describe correct cohesive energies but is constructed to give proper displacements of atoms on which a force is exerted. The vacancy formation energy obtained with this potential is not correct (1.8 eV too low). Since in this study the interest is focussed on the displacement of an atom X in a W matrix on which a repulsive force is exerted by a He atom the bulk modulus B might be the suitable parameter to look at. Under the assumption that the energy-variation of metals under volumetric changes can be described by a pair potential ϕ of the same functional form, so that the potentials can be transformed into any other by scaling the range and the potential minimum, it can be shown

that:

$$\frac{B_x}{B_w} = \frac{\eta^3}{\gamma} \qquad (4)$$

with $\eta = r_W/r_X$ and $\gamma = \phi_W^{min}/\phi_X^{min}$. With the value of η as derived from the range scaling γ can be calculated. Reynolds and Couchman [32] have used this relation with the assumption that the minimum of a pair potential is directly related to the vacancy formation energy E_V^f to demonstrate that there are three classes of metals for which the product of $B \cdot V/E_V^f$ is a constant within a class, with V the atomic volume.

Taking more recent data for the vacancy formation energy only one class can be distinguished with a few exceptions (Zn, Au, Pt). The same relation can be applied to show that $B \cdot V/E_{coh}$ should be constant, with E_{coh} the cohesive energy. Within a row of the periodic system this holds fairly well, but for totally different metals $B \cdot V/E_{coh}$ can deviate a factor two. So the accuracy of the scaling of the potential minimum will not be too good, especially for totally unlike metals.

4.2. Calculated results

In table 2 the results are shown calculated for different X–W and X–He potentials. For the X–W respectively is taken: the pure W–W potential, the W–W potential with scaled range, and the W–W potential with both range and minimum scaled. For the He–X

Table 2
Calculated binding energies E^b (eV) for He to substitutional impurities in tungsten. In set I for X–W is taken pure W–W. In set II for X–W is taken pure W–W with scaled range. In set III for X–W is taken pure W–W with scaled range and minimum. For the He–X interaction both He–X and He–X$^+$ were taken. In the last colum binding energies obtained with (5) from experimental dissociation energies are shown.

Impurity X	Set I	Set II	Set III	Experiment
Ag	0.44	0.38	0.55	0.78
Ag$^+$	0.80	0.75	0.92	
Cu	0.84	1.14	1.30	1.23
Cu$^+$	1.20	1.51	1.67	
Al	0.78	0.96	1.13	0.74
Al$^+$	1.08	1.26	1.42	
Mn	0.59	0.92	1.07	0.88
Mn$^+$	0.90	1.23	1.37	
Cr	0.70	1.00	1.12	0.77
Cr$^+$	1.06	1.36	1.49	
In	0.24	0.21	0.25	< 0.65
In$^+$	0.52	0.50	0.54	

potential two different potentials were taken, one calculated for a singly ionized X atom and one calculated for a neutral X atom.

From the table it can be learned that for most implants range scaling supplies the dominant correction to the He binding energy compared with the case that the unscaled W–W potential is taken for the W–X interaction. In the last colum of the table the experimentally measured dissociation energies are shown. The relation between dissociation energy E^d and binding energy E^b is mostly assumed to be:

$$E^d = E^b + E^m \qquad (5)$$

with E^m the migration energy. In tungsten the migration energy of He was calculated to be $E_{He}^m = 0.25$ eV by ref. [21]. To test the validity of eq. (5) for our case calculations were performed applying the He–Ag$^+$ potential of He, migrating away from a substitutional Ag atom. In fig. 8 the migration path and corresponding energy variations of the crystallite are shown. The W atoms and the Ag atom were allowed to relax fully, with the He atom held fixed at various positions. The results point out that the first energy barrier is 0.15 eV higher than the binding energy. For Cu$^+$ this figure was 0.24
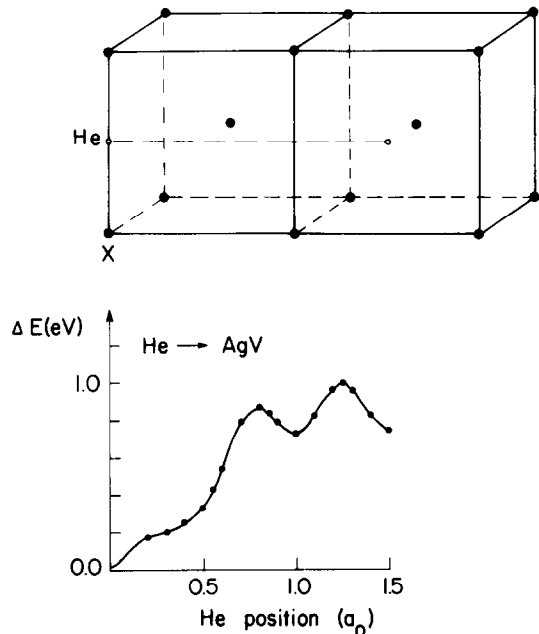

Fig. 8. Calculated energy variation of a microcrystallite ($13 \times 13 \times 13$ a_0^3) upon dissociation of a He–AgV complex, the microcrystallite was allowed to relax fully with the He atom fixed at various positions along the indicated line.
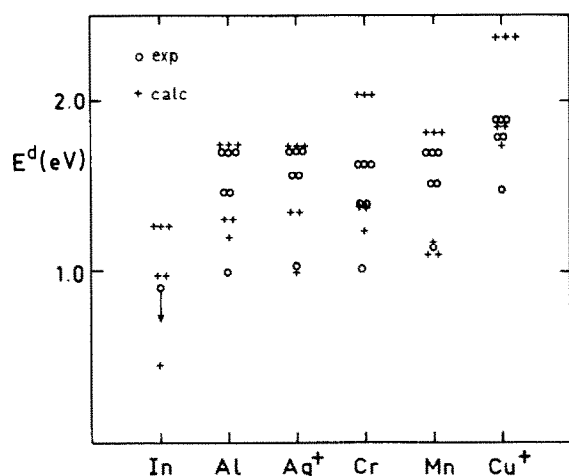
Fig. 9. Dissociation energies for He from substitutional impurities in tungsten, open circles are experimentally obtained, plusses are calculated. The number of circles c.q. plusses indicates the number of He atoms concerned.

eV, therefore it seems to be justified to compare the measured dissociation energies minus 0.25 eV directly with the calculated He binding energies. In doing so (table 2) it seems that the calculated energies agree fairly well with the measured ones presumed that He-X^+ is taken for X = Ag, Cu, and that the W-X potential is obtained by scaling the range of the W-W potential. It should be noted that in the original work in which the method of calculating the He-X potential is described for X = Ag, Cu or Au also the singly ionized X atom was taken, see ref. [21]. Bearing in mind the large uncertainty in the accuracy of the scaling of the potential minimum it is not surprising that this scaling tends to overestimate the relaxation of the impurity atoms, the more so since some relaxation effects are already incorporated due to the volume correction for charge transfer. In fig. 9 calculated dissociation energies are compared with measured ones for up to three He per trap. The trends are reproduced.

5. Discussion

Binding of He to substitutional metallic impurities in tungsten is observed. The binding energies for the first He atom are as high as 1.25 eV depending on the implant. The rather interesting point is that chromium in tungsten binds He with 0.77 eV. Cr and W have a mutual though limited solubility in each other at room

temperature, above 1800 K a complete series of solid solutions exists, as reported by Greenaway [33]. Thus this result strongly suggests that in alloys relatively strong binding of He to one of the species may occur at room temperature.

It should be realized however that tungsten is one of the most favourable metals for observing He binding to impurities since the interstitial He formation energy is rather high (> 5 eV) due to the high interatomic electron density [34]. Implants with lower electron densities than tungsten will bind He. Although hidden in the pair-potential approach the model described is based on the local electron density. The latter depends on the impurity and the possibility for the impurity to relax in the vacancy under influence of a He atom. Calculations on He-metal interactions were recently performed by Manninen et al. [34,35] for the 3d metals, using a different calculation scheme. It is interesting to note that they found a He-Mn repulsion weaker than the He-Cr repulsion. They ascribed this to magnetic effects of Mn. The He-Mn potential calculated with the modified Wedepohl method is more repulsive than the He-Cr potential calculated with this method. In the experiments the findings of ref. [34] are reproduced; the He-Mn interaction is weaker, resulting in a stronger binding of He to substitutional Mn than to Cr.

The calculations suggest that Ag and Cu transferred considerably more charge to the tungsten atoms than the implants Mn, Cr and Al.

6. Application

A possible application of the finding in this study that the He interaction with metallic impurities in metals can be understood in terms of local electron densities can be the calculation of the behaviour of He in alloys. The most obvious problem is the behaviour of He in the first wall of a fusion reactor. The first wall limiting the plasma will probably be a stainless steel alloy, containing precipitates and transmutation products, see ref. [35]. For stainless steel (SS 316) the He-X interaction functions were calculated for the different alloying elements Fe, Ni, Cr, Mn and Ti, see fig. 10. Relaxation effects will play a smaller role since atomic volume and compressibility of the constituents are similar except for Ti. The He-metal separation will be approximately $0.54a_0$, (see ref. [21]) which corresponds with 1.9 Å. At this separation the He-X interaction potentials only differ 0.1 eV, thus it will only result in a slightly higher effective He migration energy than in pure Ni.

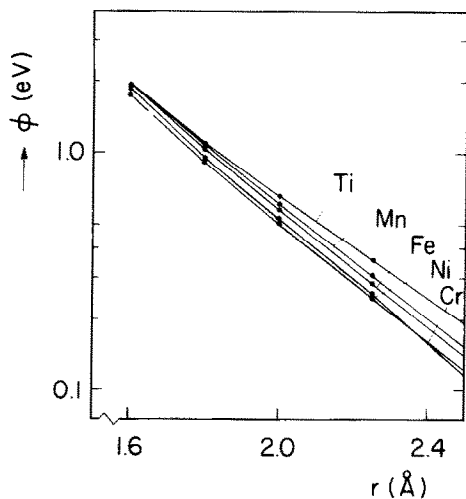For precipitates a totally different picture holds. We

Fig. 10. He-metal potentials in the intermediate region.

may expect that the minimum binding energy of He to a precipitate in SS 316 equals the difference in interstitial formation energy of He in Ni or Fe and the corresponding energy in the precipitate. Manninen et al. [34,35] calculated the heat of solution for He in 3d transition metals. From their results we expect that the binding energy of one He atom to a Ti precipitate in Fe is about 1 eV. Due to the large size mismatch the electron density at the interface will locally be considerably lower, resulting in an enhanced binding. Experimentally strong He binding has been observed to TiC precipitates in SS 316, see [37].

References

[1] A. van Veen, A.J.H. Evans, W.T.M. Buters and L.M. Caspers, Radiation Effects, to be published.
[2] J.H. Evans, A. van Veen and L.M. Caspers, Scripta Met. 17 (1983) 549.
[3] E.V. Kornelsen, Radiation Effects 13 (1972) 227.
[4] A. van Veen, L.M. Caspers, E.V. Kornelsen, R. Fastenau and A. van Gorkum, Phys. Status Solidi A40 (1977)235.
[5] D. Edwards Jr. and E.V. Kornelsen, Surface Sci. 44 (1974) 1.
[6] S.E. Donnelly, Vacuum 28 (1978) 163.
[7] E.V. Kornelsen and A.A. van Gorkum, J. Nucl. Mater. 92 (1980) 79.
[8] M. Ulrickson, J. Nucl. Mater. 85/86 (1979) 231.
[9] A. van Veen, A. Warnaar and L.M. Caspers, Vacuum 30 (1980) 109.
[10] G.J. van der Kolk, A. van Veen, L.M. Caspers and J.Th.M. de Hosson, Radiation Effects 71 (1983) 109.
[11] G.J. van der Kolk, K. Post, A. van Veen, F. Pleiter and J.Th.M. de Hosson, Radiation Effects, to be published.
[12] A.A. van Gorkum and E.V. Kornelsen, Radiation Effects 42 (1979) 93.
[13] E.V. Kornelsen and A.A. van Gorkum, Radiation Effects 42 (1979) 113.
[14] G.J. van der Kolk, A. van Veen, J.Th.M. de Hosson and R.H.J. Fastenau, Nucl. Instrum. Methods, to be published.
[15] E.V. Kornelsen and M.K. Shinha, J. Appl. Phys. 39 (1968) 4546.
[16] D.K. Sood, Phys. Letters 68A (1978) 469.
[17] W. Gordy, Phys. Rev. 69 (1946) 604.
[18] A. van Veen W.Th.M. Buters, G.J. van der Kolk, L.M. Caspers and T.R. Armstrong, Nucl. Instrum. Methods 194 (1982) 485.
[19] A. van Veen, W.Th.M. Buters, T.R. Armstrong, B. Nielsen, K.T. Westerduin, L.M. Caspers and J.Th.M. de Hosson, Nucl. Instrum. Methods 209/210 (1983) 1055.
[20] A. Wagner and D.N. Seidman, Phys. Rev. Letters 42 (1979) 515.
[21] W.D. Wilson and R.A. Johnson, in: Interatomic Potentials and Simulation of Lattice Defects, Eds. P.C. Gehlen, J.R. Beeler jr. and R.I. Jaffee (Plenum Press, New York, 1972) p. 375.
[22] J.Th.M. de Hosson, in: Interatomic Potentials and Crystalline Defects, Ed. J.K. Lee (Michigan, 1981) p. 3.
[23] R.A. Johnson and W.D. Wilson, ibid. [13] p. 301.
[24] M. Baskes, private communication.
[25] P.T. Wedepohl, Proc. Phys. Soc. 92 (1967) 79.
[26] W.D. Wilson and C.L. Bisson, Phys. Rev. B3 (1971) 3984.
[27] F. Herman and S. Skillman, Atomic Structure Calculations (Prentice Hall Inc, New Jersey, 1963).
[28] E.M. Machlin, Acta. Metall. 22 (1974) 109, 22 (1974) 367, 22 (1974) 1433.
[29] E.M. Machlin, in: Theory of Alloy Phase Formation, Ed. L.H. Bennett (New Orleans, 1979) p. 127.
[30] K. Maeda, V. Vitek and P. Sutton, Acta. Metall. 30 (1982) 2001.
[31] V. Vitek and Y. Minonishi, Surface. Sci., to be published.
[32] C.L. Reynolds and J.R. Couchman, Phys. Letters. 50A (1974) 157.
[33] H.T. Greenaway, J. Inst. Metals 80 (1951, 1952) 589.
[34] M. Manninen, J.K. Norskov and C. Umrigar, J. Phys. F12 (1982) L7.
[35] M.J. Puska, R.M. Nieminen and M. Manninen, Phys. Rev. B24 (1981) 3037.
[36] R.W. Conn, J. Nucl. Mater. 103 (1981) 7.
[37] W. Kesternich and J. Rothaut, J. Nucl. Mater. 103 (1981) 845.